Multiparticle correlations in complex scattering and the mesoscopic Boson Sampling problem

Juan-Diego Urbina, Jack Kuipers, Quirin Hummel, and Klaus Richter
Institut für Theoretische Physik, Universität Regensburg, D-93040 Regensburg, Germany

We consider the many-body scattering of non-interacting identical particles in mesoscopic chaotic cavities. A complete enumeration of all interfering paths allows us to discriminate single-particle effects from many-body interference due to quantum indistinguishability. In the thermodynamic limit of large particle number massive quantum interference results in a macroscopic, coherent manifestation of many-body correlations. We also incorporate mesoscopic dephasing, present even when the particles scatter simultaneously. Under further simplifications characteristic for optical scenarios, our methods can be used to address open issues related to the Boson Sampling problem.

PACS numbers: 03.65.Sq, 05.45.Mt, 42.50.Ar, 73.23Ad

In quantum mechanics, the symmetrization postulate makes it impossible to characterize systems of identical particles by labeling their constituents individually: identical particles are indistinguishable and their very identity is then affected by quantum fluctuations and interference effects. In open (scattering) systems, where one is interested in processes connecting incoming to outgoing states describing several particles, the transition probabilities are given by a mixture of Single-Particle (SP) and Many-Body (MB) effects. By definition, the former are already present in the wave scattering of a single particle, while MB effects are due to interparticle forces and quantum indistinguishability. Remarkably, and in sharp contrast with interactions, indistinguishability does not have a classical limit, and therefore its observable consequences provide a hallmark of genuine quantum MB coherence.

A prominent type of MB correlations is exemplified by the celebrated Hong-Ou-Mandel (HOM) effect [1], by now the standard indicator of MB coherence in quantum optics. There, the probability of observing two photons leaving simultaneously in different arms of a beam splitter is measured. As a function of the delay between the arrival of the incoming photons into the beam splitter, the coincidence probability shows a characteristic dip in agreement with theoretical expectations [1]. The study of MB correlations due to indistinguishability has been a focus of intense scrutiny, with a wealth of hallmark experimental studies of MB scattering of identical particles that have attempted to leave the classic HOM scenario by increasing the number of particles and/or the complexity of the scattering process [2–6]. So far, however, theoretical approaches have assumed that already at the SP level the scattering process is itself perfectly known and independent of the characteristics of the incoming state [7–13]. In the mesoscopic scenario depicted in Fig. 1 where the scattering region Ω is a physical cavity, however, this is not the case as the SP scattering process strongly depends of the cavity's geometry and the energy of the incoming particles. Moreover, a generic cavity is non-integrable, and the mesoscopic MB scattering problem is naturally described within a statistical approach.

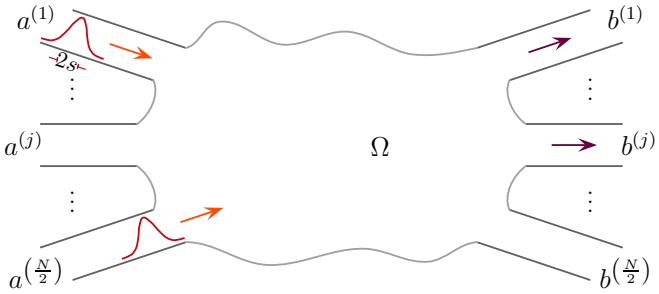

FIG. 1. Many-body scattering of non-interacting indistinguishable particles. Identical wavepackets with shifted mean position along the leads are scattered by the irregular cavity.

In this paper we present analytic results on properties of MB correlations in the mesoscopic regime. Supported by the universal correlations of SP scattering matrices [14] responsible for characteristic mesoscopic effects like weak localization [15] and universal conductance fluctuations [16], here we address the emergence of universal MB correlations due to the interplay between classical ergodicity, SP interference and quantum indistinguishability well beyond standard semiclassical SP pictures [17]. Surprisingly, and despite their intrinsically non-classical character, MB correlations are here successfully explained and computed within a semiclassical approach in terms of interfering SP classical paths in the spirit of the Feynman path integral [18] by providing a one-to-one correspondence between MB classical paths (illustrated in Fig. 2) and terms of the expansion of the MB scattering probabilities. Our complete enumeration and classification of the MB paths allows for an explicit analysis of emergent phenomena in the thermodynamic many-particle limit, something out of reach of leading-order random matrix techniques [19–21]. Moreover, we show that the cavity's dwell time, a physical parameter characteristic of the mesoscopic regime, drastically af-

fects the HOM effect leading eventually to a universal exponential profile.

Although we present results for both massive bosons and fermions scattered by cavities including all SP and MB interference mechanisms, our methods can be readily extended to the optical case by both using the dispersion relation for photons and neglecting mesoscopic SP effects. To make connection to corresponding experiments [7–13] this amounts to replace the cavity Ω by a multi-port waveguide network. Then one finds that the dependence of the MB transition probabilities on the SP scattering matrix σ is of purely combinatorial origin. Aaronson and Arkhipov proved that already in this simplified limit, the complexity of this dependence for a given fixed σ suffices to make the calculation of MB transition probabilities a computationally hard task, the so-called Boson Sampling (BS) problem [22]. Our results shed light on timely questions like the thermodynamic limit of BS and show the dynamical origin of the uniform distribution in Hilbert space, an object of ubiquitous presence in BS and related problems like the Bosonic birthday paradox [23].

The set up of the mesoscopic many-body scattering problem is depicted in Fig. 1. The incoming particles ($i=1,\ldots,n$) with positions (x_i, y_i) occupy single-particle states represented by normalized wavepackets

$$\phi_i(x_i, y_i) \propto \mathrm{e}^{-ik_i x_i} X_i(x_i - z_i)\chi_{a_i}(y_i)\,. \tag{1}$$

The longitudinal wavepacket $X_i(x_i - z_i)$ of the ith particle has variance s_i^2, mean initial position $z_i \gg s_i$, and approaches the cavity Ω with mean momentum $\hbar k_i = mv_i > 0$ along the longitudinal direction $-x_i$. The transverse wavefunction in the incoming channel $a_i \in \{a^{(1)}, \ldots, a^{(N/2)}\}$ is $\chi_{a_i}(y_i)$ and has energy E_{a_i}. Although a general treatment is possible, we will assume that, except for their relative positions parametrized by $z_{ij} = z_i - z_j$, the wavepackets and initial transversal modes are identical: $s_i = s$, $\hbar k_i = \hbar k = mv$, and $E_{a_i} = E_{\mathrm{ch}}$ for all i.

The joint probability to find n particles leaving in channels $\mathbf{b}=(b_1,\ldots,b_n)$ with energies $\mathbf{E}=(E_1,\ldots,E_n)$, after entering the cavity in channels $\mathbf{a}=(a_1,\ldots,a_n)$ is given by

$$P_{\mathbf{a},\mathbf{b}} = \int_{E_{\mathrm{ch}}}^{\infty} |A_{\mathbf{a},\mathbf{b}}(\mathbf{E})|^2 dE_1 \ldots dE_n\,, \tag{2}$$

in terms of the $\mathbf{E}$-dependent n-particle amplitude [24]

$$A_{\mathbf{a},\mathbf{b}}(\mathbf{E}) = \prod_{i=1}^{n} \frac{\mathrm{e}^{-i(k-k_{\mathrm{ch}}(E_i))z_i}}{\sqrt{\hbar v_{\mathrm{ch}}(E_i)}} \tilde{X}(k - k_{\mathrm{ch}}(E_i))\sigma_{b_i,a_i}(E_i)\,. \tag{3}$$

When $n = 1$, Eq. (3) formally defines the SP scattering matrix $\sigma_{b,a}(E)$ connecting the incoming and outgoing channels a and b. We also have $\hbar k_{\mathrm{ch}}(E) = mv_{\mathrm{ch}}(E) = \sqrt{2m(E - E_{\mathrm{ch}})}$ and $\tilde{X}(k) = (1/\sqrt{2\pi}) \int_{-\infty}^{\infty} \mathrm{e}^{-ikx} X(x)dx$. Note that the transition probability for distinguishable particles, $P_{\mathbf{a},\mathbf{b}}$, is insensitive to the relative positions of the incoming wavepackets z_{ij}.

If the particles are identical, quantum indistinguishability demands their joint state to be symmetrized according to their spin [25]. Introducing $\epsilon = -1$ $(+1)$ for fermions (bosons), the symmetrized amplitude is given by a sum over the $n!$ elements $\mathcal{P}$ of the permutation group,

$$A^{(\epsilon)}_{\mathbf{a},\mathbf{b}}(\mathbf{E}) = \sum_{\mathcal{P}} \epsilon^{\mathcal{P}} A_{\mathbf{a},\mathcal{P}\mathbf{b}}(\mathcal{P}\mathbf{E})\,. \tag{4}$$

We further introduce

$$\int^{<} d\mathbf{E}\ (\cdot) = \int_{E_{\mathrm{ch}}}^{\infty} dE_1 \int_{E_{\mathrm{ch}}}^{E_1} dE_2 \ldots \int_{E_{\mathrm{ch}}}^{E_{n-1}} dE_n\ (\cdot)\,, \tag{5}$$

to avoid the double counting implicit in the identification of the many-body states $|\mathbf{E}, \mathbf{a}\rangle$ and $|\mathcal{P}\mathbf{E}, \mathcal{P}\mathbf{a}\rangle$. For simplicity, in Eq. (5) we assumed that the output channels are open if the incoming are, $E_{b_i} \leq E_{\mathrm{ch}}$. Then

$$P^{(\epsilon)}_{\mathbf{a},\mathbf{b}} = \int^{<} |A^{(\epsilon)}_{\mathbf{a},\mathbf{b}}(\mathbf{E})|^2 d\mathbf{E} = P^{\mathrm{inc}}_{\mathbf{a},\mathbf{b}} + P^{\mathrm{int}}_{\mathbf{a},\mathbf{b}}\,, \tag{6}$$

defines the MB transition probability that is naturally separated into an incoherent contribution

$$P^{\mathrm{inc}}_{\mathbf{a},\mathbf{b}} = \sum_{\mathcal{P}} \int^{<} |A_{\mathbf{a},\mathcal{P}\mathbf{b}}(\mathcal{P}\mathbf{E})|^2 d\mathbf{E}\,, \tag{7}$$

and a MB term due to interference between different distinguishable MB configurations

$$P^{\mathrm{int}}_{\mathbf{a},\mathbf{b}} = 2n!\Re \sum_{\mathcal{P}\neq \mathrm{id.}} \epsilon^{\mathcal{P}} \int^{<} d\mathbf{E} A_{\mathbf{a},\mathcal{P}\mathbf{b}}(\mathcal{P}\mathbf{E}) A^{*}_{\mathbf{a},\mathbf{b}}(\mathbf{E})\,. \tag{8}$$

The later depends on the offsets z_{ij} that allow for tuning the strength of the interference through dephasing, and thereby can be heuristically understood as sensitive to the degree of indistinguishability itself [5, 6].

The original HOM scenario [1] corresponds to $N = 4, n = 2$ and σ energy independent. We get

$$P^{\mathrm{HOM}}_{\mathbf{a},b_1\neq b_2} = \frac{|\mathrm{Per}(\sigma)|^2 + 1}{4} + \epsilon \frac{|\mathrm{Per}(\sigma)|^2 - 1}{4}\ \mathcal{F}^2(z_{12}) \tag{9}$$

using Eqs. (4) and (6), with Per denoting the permanent (unsigned determinant), and the overlap integral

$$\mathcal{F}(z) = \int_{-\infty}^{\infty} X(x)X(x - z)dx\,. \tag{10}$$

Individual σ-matrices with specific entries leading to Eq. (9) and its many-particle generalizations are routinely constructed in arrays of beam splitters connecting waveguides for photonic systems [8, 9, 12, 13] and through quantum point contacts for electrons occupying edge states [26, 27]. If the beam splitter or point

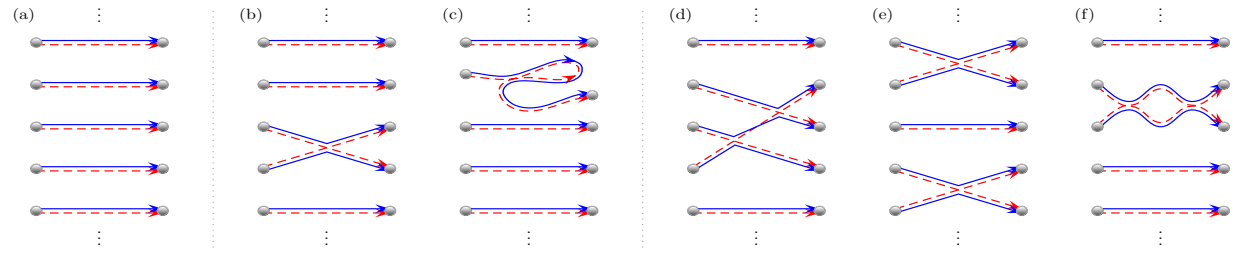

FIG. 2. Many-body (MB) paths contributing to the single-particle (SP) scattering matrix correlations required for calculating of transition probabilities. In (a), both SP and MB correlations are neglected. In (c), weak localization at the SP level is included. For (b,d,e), and (f) only MB correlations are included. Combined SP and MB effects appear when the links in a MB diagram are decorated with SP loops.

contact is replaced by a mesoscopic cavity, acting as a complex scatter, additional time scales are introduced, and thereby further physical effects enter into the problem. Perfect control of σ is neither feasible, nor necessary to address observables averaged over energy windows or variations of the geometry of the cavity. In the semiclassical regime of short wavelengths it is an established fact that for complex scattering where the classical dynamics is chaotic, products of the form $\sigma_{b,a}(E)\sigma^*_{b',a'}(E')$ display universal features under average, depending only on the presence or absence of time reversal invariance, denoted as the orthogonal ($\beta = 1$) and unitary ($\beta = 2$) case [14–16, 28]. Universal interference effects in the scattering probabilities are semiclassically understood in terms of statistical correlations among classical actions [14–16, 29].

From Eqs. (3, 4) the average $\langle |A^{(\epsilon)}_{\mathbf{a},\mathbf{b}}(\mathbf{E})|^2\rangle$ of the transition probabilities over an ensemble of σ-matrices involves higher-order correlations and different energies. Our semiclassical calculation of σ-matrix correlations is depicted in Fig. 2 for the case of interest here where $b_i \neq b_{j\neq i}, b_i \neq a_j$ and $a_i \neq a_j$ for all i, j. A $2n$-order correlator of σ-matrices is given by an infinite diagrammatic expansion with terms that can be visualized as a set of links joining n incoming and outgoing channels. The classical transition probability,

$$\langle P^{\rm class}_{\mathbf{a},\mathbf{b}}\rangle = N^{-n}\,, \tag{11}$$

is obtained from the trivial topology in Fig. 2(a). In Eq. (11) N is the number of open channels at the mean energy $U = mv^2/2 + E_{\rm ch}$ of the incoming particles. Quantum effects at the SP level are generated by adding SP loops to the links, as in Fig. 2(c) and can be evaluated up to infinite order to give

$$\begin{aligned}\langle P^{\rm inc}_{\mathbf{a},\mathbf{b}}\rangle &= \frac{1}{N^n} - \left(\frac{2}{\beta} - 1\right)\sum_{l=1}^{\infty}\frac{(-1)^l}{N^{n+l}}\binom{n+l}{l} \\ &= (N - 1 + 2/\beta)^{-n}\,,\end{aligned} \tag{12}$$

the nth power of the SP transition probability [14, 15].

In order to calculate $P^{\rm int}$, Eq (8), we must include genuine MB effects characterized by correlations between different SP paths. With an obvious notation, the first MB diagrams without SP loops depicted in Fig. 2 are labeled by $\{2\}$ (b), $\{3\}$ (d), $\{2,2\}$ (e) while Fig. 2(f) shows the diagram $\{2\}$ with a loop between 2 particles.

The basic correlator $\{2\}$ in Fig. 2(b) involving a single pair of correlated paths is [16, 30]

$$\begin{aligned}&\langle \sigma_{b_i,a_i}(E_i)\sigma_{b_j,a_j}(E_j)\sigma^*_{b_i,a_j}(E_j)\sigma^*_{b_j,a_i}(E_i)\rangle \\ &\quad = \frac{1}{N^3}\frac{\hbar^2}{\hbar^2 + \tau_d^2(E_i - E_j)^2} + \mathcal{O}(1/N^4),\end{aligned} \tag{13}$$

where τ_d is the dwell time, the average time a particle with energy $(E_i + E_j)/2$ remains within Ω before exiting through the leads. Eqs. (8) and (3) give [31]

$$\langle P^{\rm int}_{\mathbf{a},\mathbf{b}}\rangle^{\{2\}} = -\frac{\epsilon}{N^{n+1}}\sum_{i<j}\mathcal{Q}^{(2)}(z_{ij})\,, \tag{14}$$

with the generalization of the overlap integral Eq. (10),

$$\mathcal{Q}^{(2)}(z) = \int_{-\infty}^{\infty}\mathcal{F}^2(z - vt)\frac{\mathrm{e}^{-\frac{|t|}{\tau_d}}}{2\tau_d}dt\,. \tag{15}$$

The functions $\mathcal{Q}^{(2)}$ determine how the MB correlations decay when the delay times $\tau_{ij} = z_{ij}/v$ entering $\mathcal{F}$ increase. We interpret Eq. (15) as follows: Pairs of incoming particles that are effectively distinguishable get to interfere if their time delay τ_{ij} in entering the cavity is compensated by the time τ_d the first particle is held within the mesoscopic scattering region. However, the interference gets weighted by the survival probability $\mathrm{e}^{-t/\tau_d}/\tau_d$ of remaining inside the chaotic scatter Ω.

Universality of the dephasing of MB correlations is expected if τ_d competes with the delay times τ_{ij} and widths $\tau_s = s/v$ of the incoming wavepackets. Universal exponential tails in the interference profile for $|z_{ij}| \gg s$ can be made explicit if we assume that the overlap $\mathcal{F}(x)$ decays faster than exponentially to give $\mathcal{Q}^{(2)}(z \gg s) \sim \mathrm{e}^{-|z|/v\tau_d}$. As shown in Fig. 3, the region of exponential tails grows with the ratio τ_d/τ_s. We can thus identify a universal regime where the suppression of MB interference is exponential

$$\mathcal{Q}^{(2)}(z) \xrightarrow{v\tau_d \gg v\tau_s \gg 1/k} \mathcal{C}^{(2)}\frac{\tau_s}{2\tau_d}\mathrm{e}^{-\frac{|z|}{v\tau_d}}\,, \tag{16}$$

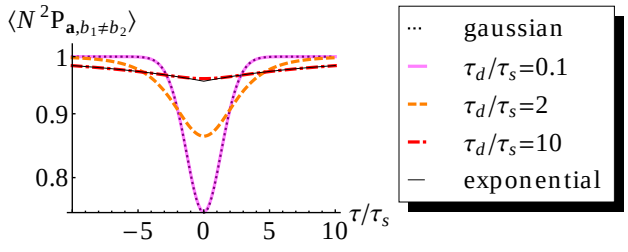

FIG. 3. Overlapping (Gaussian due the shape of the incoming wavepackets) and universal (exponential) regimes for the mesoscopic HOM interference profile, depicting the probability of finding two bosons in different exit channels.

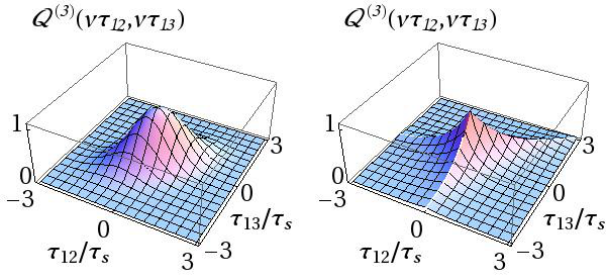

FIG. 4. Transition between the overlapping ($\tau_d/\tau_s = 0.1$, left) and the universal exponential ($\tau_d/\tau_s = 10$, right) regime for the three-body interference term, Eq. (18).

with $\mathcal{C}^{(2)} = s^{-1}\int_{-\infty}^{\infty}\mathcal{F}^2(z)dz$. In the opposite regime, we observe a non-universal result

$$\mathcal{Q}^{(2)}(z) \xrightarrow{v\tau_s\gg v\tau_d>1/k} \mathcal{F}^2(z)\,. \tag{17}$$

Here the interference profile depends, as in the optical HOM effect Eq. (9), on the shape of the incoming wavepackets. These observations are not particular to two-body interference. The diagram Fig. 2(d) containing three-body correlations (the mesoscopic analogue of the correlations measured in [6]) gives

$$\langle P^{\rm int}_{\mathbf{a},\mathbf{b}}\rangle^{\{3\}} = \frac{2\epsilon}{N^{n+2}}\sum_{i<j<k}\mathcal{Q}^{(3)}(z_{ij},z_{kj})\,, \tag{18}$$

with regimes shown in Fig. 4 and given by

$$\mathcal{Q}^{(3)}(z,z')\begin{cases}\xrightarrow{v\tau_d\gg v\tau_s\gg 1/k} & \mathcal{C}^{(3)}\,\mathrm{e}^{-\frac{3\mathrm{Max}(z,z',0)}{v\tau_d}}\,\mathrm{e}^{\frac{z+z'}{v\tau_d}}\\ \xrightarrow{v\tau_s\gg v\tau_d>1/k} & \mathcal{F}(z)\mathcal{F}(z')\mathcal{F}(z-z')\end{cases}, \tag{19}$$

with $\mathcal{C}^{(3)} = s^{-2}\int_{-\infty}^{\infty}\mathcal{F}(z)\mathcal{F}(z')\mathcal{F}(z-z')dzdz'$.

As the main application however, we address the fate of MB interference effects due to indistinguishability in the thermodynamic limit $N, n\to\infty$, a fundamental issue of present interest [2, 22, 23, 32, 33]. The expansion of the correlators in powers of N^{-1}, Eqs. (11,14,18) must be reconsidered in view of the fast (combinatorial) growth (with n) of the number of MB terms in each diagram. For a well defined thermodynamic limit we need a proper scaling $N = \alpha n^\eta$ to control asymptotically large diagrams. It can be shown order by order [31] that loop contributions are of higher order and the dominant contributions are of the form $\{2\}, \{2,2\}, \{2,2,2\}, \ldots$, obtained by simple pairwise correlations among links. Using Eq. (13), all pairwise diagrams can be evaluated in closed form giving

$$\langle P^{\rm int}_{\mathbf{a},\mathbf{b}}\rangle^{\{2,2\}} = \frac{\epsilon^2}{N^{n+2}}\sum_{(i,i')<(j,j')}\mathcal{Q}^{(2)}(z_{ij})\mathcal{Q}^{(2)}(z_{i'j'}) \tag{20}$$

and the obvious generalization for arbitrary orders.

We specifically consider now the case $z_{ij} = 0$ where all the particles are injected at the same mean position and where we expect the peak of the interference profile. All contributions which are not made up from pairs of correlated trajectories vanish for $n \gg 1$, while from the sum of the pairwise diagrams we easily get

$$\frac{\langle P^{(\epsilon)}_{\mathbf{a},\mathbf{b}}\rangle_{z_{ij}=0}}{\langle P^{\rm class}_{\mathbf{a},\mathbf{b}}\rangle} \xrightarrow{n\gg 1} \sum_{l=0}^{[n/2]}\left(\frac{-\epsilon\mathcal{Q}^{(2)}(0)}{N}\right)^l (2l-1)!!\binom{n}{2l}\,. \tag{21}$$

By inspection of the series we find that the proper scaling giving a finite, non-zero thermodynamic limit must be $\eta = 2$, and we obtain finally

$$\left.\frac{\langle P^{(\epsilon)}_{\mathbf{a},\mathbf{b}}\rangle_{z_{ij}=0}}{\langle P^{\rm class}_{\mathbf{a},\mathbf{b}}\rangle}\right|_{N=\alpha n^2} \xrightarrow{n\to\infty} \mathrm{e}^{-\epsilon\mathcal{Q}^{(2)}(0)/2\alpha}\,. \tag{22}$$

Equation (22) shows that under ensemble average and a proper scaling, in the universal limit MB interference due to indistinguishability produces macroscopic statistical effects. More importantly, following well established results in the field of quantum chaos [34], *it is expected that for Eq. (22) to hold in chaotic systems it is enough to perform averages over small variations of the system parameters.* The quadratic scaling $N = \alpha n^2$ has been noted before [22, 32, 33], and it is related with the so-called bosonic birthday paradox [23]. Within our dynamical approach it is supported by the conjecture [31]

$$\frac{\langle P^{(\epsilon)}_{\mathbf{a},\mathbf{b}}\rangle^{\tau_d=0}_{z_{ij}=0}}{\langle P^{\rm class}_{\mathbf{a},\mathbf{b}}\rangle} = \prod_{k=0}^{n-1}\frac{N}{N+\epsilon k}\,, \tag{23}$$

which gives the asymptotics (for $\eta \neq 2$)

$$\left.\left(\frac{\langle P^{(\epsilon)}_{\mathbf{a},\mathbf{b}}\rangle^{\tau_d=0}_{z_{ij}=0}}{\langle P^{\rm class}_{\mathbf{a},\mathbf{b}}\rangle}\right)^{\epsilon}\right|_{N=\alpha n^\eta} \xrightarrow{n\to\infty} \begin{cases}0 & \text{for}\quad 1<\eta<2\\ 1 & \text{for}\quad \eta>2\,,\end{cases}$$

showing a sharp transition between classical and quantum correlations in the thermodynamic limit.

Along with the semiclassical techniques in [31], for the case when $z_{ij} = 0$ the transition probabilities should be

amenable to random matrix approaches which could be a route to proving Eq. (23). Also in [31] we calculate the leading order of the second moment and variance of the transition probabilities. In fact, determining just the leading order of higher moments should be pertinent for the *Permanent Anti-Concentration Conjecture* important for BS [22]. Intriguingly then, semiclassical diagrams and random matrices open up new avenues for understanding permanent statistics.

In conclusion, we have presented a semiclassical theory of mesoscopic many-body scattering of non-interacting, identical particles based on interfering single-particle trajectories. We have shown the existence of a universal regime where massive interference due to chaotic scattering leads to quantum indistinguishability effects that survive in the thermodynamic limit, providing a dynamical basis for recent statistical approaches to the Boson-Sampling problem. We also show that if the typical time τ_d a particle remains in the scattering region is finite, the HOM profile universally displays exponential (instead of Gaussian) tails, thus extending the regime where many-body correlations can be detected. Finally, in the limit $\tau_d = 0$, our methods can be used to describe mode correlation functions in random optical arrays where other type of MB correlations can play a role.

We want to thank Andreas Buchleitner and Malte Tichy for instructive discussions, and Markus Birberger for his help in preparing the mansucript.

[1] C. K. Hong, Z. Y. Ou, and L. Mandel, *Phys. Rev. Lett.* **59**, 2044 (1987).

[2] M. Tillmann, B. Dakic, R. Heilmann, S. Nolte, A. Szameit, and P. Walther, *Nature Photon.* **7**, 540 (2013).

[3] M. A. Broome, A. Fedrizzi, S. Rahimi-Keshari, J. Dove, S. Aaronson, T. C. Ralph, and A. G. White, *Science* **339**, 794 (2013).

[4] A. Crespi, R. Osellame, R. Ramponi, D. J. Brod, E. F. Galvao, N. Spagnolo, C. Vitelli, E. Maiorino, P. Mataloni, and F. Sciarrino, *Nature Photon.* **7**, 545 (2013).

[5] Y.-S. Ra, M. C. Tichy, H.-T. Lim, O. Kwon, F. Mintert, A. Buchleitner, and Y.-H. Kim, *Nature Commun.* **4**, (2013).

[6] M. Tillmann, S.-H. Tan, S. E. Stoeckl, B. C. Sanders, H. de Guise, R. Heilmann, S. Nolte, A. Szameit, and P. Walther, *Boson Sampling with Controllable Distinguishability* arXiv:1403.3433 (2014).

[7] M. C. Tichy, M. Tiersch, F. de Melo, F. Mintert, and A. Buchleitner, *Phys. Rev. Lett.* **104**, 220405 (2010).

[8] S. Aaronson and A. Arkhipov, *Boson sampling is far from uniform* arXiv:1309.7460 (2013).

[9] P. P. Rhode, K. R. Motes, and J. P. Dowling, *Sampling generalized cat states with linear optics is probably hard* arXiv:1310.0297 (2013).

[10] C. Gogolin, M. Kliesch, L. Aolita, and J. Eisert, *Boson-sampling in the light of sample complexity* arXiv:1306.3995 (2013).

[11] V. S. Shchesnovich, *Phys. Rev. A* **89**, 022333 (2014).

[12] J. B. Spring, B. J. Metcalf, P. C. Humphreys, W. S. Kolthammer, X.-M. Jin, M. Barbieri, A. Datta, N. Thomas-Peter, N. K. Langford, D. Kundys, J. C. Gates, B. J. Smith, P. G. R. Smith, and I. A. Walmsley, *Science* **339**, 798 (2013).

[13] B. J. Metcalf, N. Thomas-Peter, J. B. Spring, D. Kundys, M. A. Broome, P. Humphreys, X.-M. Jin, M. Barbieri, W. S. Kolthammer, J. C. Gates, B. J. Smith, N. K. Langford, P. G. R. Smith, and I. A. Walmsley, *Nature Comm.* **4**, 1356 (2013).

[14] G. Berkolaiko and J. Kuipers, *Phys. Rev. E* **85**, 045201 (2012); *J. Math. Phys.* **54**, 112103 (2013).

[15] K. Richter and M. Sieber, *Phys. Rev. Lett.* **89**, 206801 (2002).

[16] S. Müller, S. Heusler, A. Altland, P. Braun, and F. Haake, *New J. Phys.* **11**, 103025 (2009).

[17] See for example R. K. Badhuri and M. Brack *Semiclassical Physics*, Addison-Wesley (Reading) 1997.

[18] L. S. Schulman, *Techniques and Applications of Path Integration*, John Wiley & Sons (New York) 1981; M. Gutzwiller, *Chaos in Classical and Quantum Mechanics*, Springer Verlag (New York) 1990.

[19] C. W. J. Beenakker, J. W. F. Venderbos, and M. P. van Exter, *Phys. Rev. Lett.* **102**, 193601 (2009).

[20] M. Cand and S. E. Skipetrov, *Phys. Rev. A* **87**, 013846 (2013).

[21] M. Cand, A. Goetschy, and S. E. Skipetrov, *Transmission of quantum entanglement through a random medium* arXiv:1406.7202 (2014).

[22] S. Aaronson and A. Arkhipov, STOC '11 43rd ann. ACM *Symp. Theo. Comp.* **333**, (2011).

[23] A. Arkhipov and G. Kuperberg, *Geom. and Topol. Mon.* **18**, 1 (2012).

[24] S. Weinberg, *The quantum theory of fields* Cambridge University Press (NY) 2005; M. Gell-Mann and M. L. Goldberger, *Phys. Rev.* **91**, 398 (1953).

[25] J. J. Sakurai, *Modern Quantum Mechanics*, Addison-Wesley (Reading) 1967.

[26] E. Bocquillon, V. Freulon, F. D. Parmentier, J.-M. Berroir, B. Placais, C. Wahl, J. Rech, T. Jonckheere, T. Martin, C. Grenier, D. Ferraro, P. Degiovanni, and G. Feve, *Annalen der Physik* **526**, 1 (2014).

[27] C. W. J. Beenakker, C. Emary, M. Kindermann, and J. L. van Velsen, *Phys. Rev. Lett.* **91**, 147901 (2003).

[28] C. W. J. Beenakker, *Rev. Mod. Phys.* **69**, 731 (1997).

[29] D. Waltner, *Semiclassical approach to mesoscopic systems*, Springer-Verlag (Heidelberg) 2012.

[30] J. Kuipers and M. Sieber, *Phys. Rev. E* **77**, 046219 (2008).

[31] See supplementary material.

[32] M. C. Tichy, K. Mayer, A. Buchleitner, and K. Molmer, *Phys. Rev. Lett.* **113**, 020502 (2014).

[33] V. S. Shchesnovich, *Conditions for experimental Boson-Sampling computer to disprove the Extended Church-Turing thesis*, arXiv:1403.4459 (2014).

[34] F. Haake, *Quantum Signatures of Chaos*, Springer (Berlin) 2010.

SUPPLEMENTARY MATERIAL

CALCULATION OF $\mathcal{Q}^2(z)$

Using the definition Eq. (8) we get

$$\mathcal{Q}^{(2)}(z) = \int_{E_{\rm ch}}^{\infty} dE_1 dE_2 \frac{\mathrm{e}^{i(k_{\rm ch}(E_2)-k_{\rm ch}(E_1))z}}{1+\left[\frac{\tau_d(E_1-E_2)}{\hbar}\right]^2} \times \frac{|\tilde{X}(k-k_{\rm ch}(E_1))|^2|\tilde{X}(k-k_{\rm ch}(E_2))|^2}{\hbar^2 v_{\rm ch}(E_1)v_{\rm ch}(E_2)}\,, \tag{24}$$

where the symmetry of the integrand under interchange of E_1 and E_2 is used. To further proceed, we use $E_i = E_{\rm ch} + \hbar^2 q_i^2/2m$ and $q = q_2 - q_1, Q = (q_1+q_2)/2$. Then we observe that the momentum representation of the incoming wavepackets $\tilde{X}(q_i - k)$ are strongly localised around $q_1 = q_2 = k$. As long as $ks \gg 1$ we can extend the lower limit of integrals to $-\infty$ and keep only terms of first order in q. Under this conditions Eq. (24) yields

$$\mathcal{Q}^{(2)}(z) = \int_{-\infty}^{\infty} dQ dq \frac{\mathrm{e}^{iqz}}{1+v^2\tau_d^2 q^2} \times |\tilde{X}(Q-k-q/2)|^2|\tilde{X}(Q-k+q/2)|^2\,, \tag{25}$$

which can be finally transformed into

$$\mathcal{Q}^{(2)}(z) = \int_{-\infty}^{\infty} \mathcal{F}^2(z-vt)\frac{\mathrm{e}^{-\frac{|t|}{\tau_d}}}{2\tau_d}dt\,. \tag{26}$$

SEMICLASSICAL TREATMENT OF SCATTERING MATRIX CORRELATORS

For n bosons, we start with the expression

$$\tilde{A}_n^+ = \frac{1}{\sqrt{n!}} \sum_{\mathcal{P}\in S_n} \prod_{k=1}^{n} Z_{i_k, o_{\mathcal{P}(k)}}\,, \tag{27}$$

where we sum over all permutations $\mathcal{P}$ of $\{1,\dots,n\}$ and where $Z = \sigma^{\rm T}$ is the transpose of the single particle scattering matrix σ (so we can identify the first subscript as an incoming channel and the second as an outgoing one). For simplicity we assume that all the channels are distinct. This quantity is related to the n-particle amplitude when the particle energies coincide or $\tau_d = 0$.

We will treat correlators of A_n using a semiclassical approach. This is heavily based on [35–38] and we refer in particular to [35, 37] for the underlying details and methods.

Transmission probabilities

First we are interested in

$$|\tilde{A}_n^+|^2 = \tilde{A}_n^+(\tilde{A}_n^+)^* = \frac{1}{n!}\sum_{\mathcal{P},\mathcal{P}'\in S_n}\prod_{k=1}^{n} Z_{i_k,o_{\mathcal{P}(k)}} Z^*_{i_k,o_{\mathcal{P}'(k)}}\,. \tag{28}$$

The averages over scattering matrix elements are known both semiclassically and from RMT (see [37, 39] for example)

$$\left\langle Z_{a_1,b_1}\cdots Z_{a_n,b_n} Z^*_{\alpha_1,\beta_1}\cdots Z^*_{\alpha_n,\beta_n}\right\rangle = \sum_{\sigma,\pi\in S_n} V_N(\sigma^{-1}\pi)\prod_{k=1}^{n}\delta(a_k-\alpha_{\sigma(k)})\delta(b_{\bar{k}}-\beta_{\pi(\bar{k})})\,, \tag{29}$$

where V are class coefficients which can be calculated recursively.

However, since the channels are distinct, for each pair of permutations $\mathcal{P},\mathcal{P}'$ in Eq. 28 only the term with $\sigma = id$ and $\pi = \mathcal{P}(\mathcal{P}')^{-1}$ in Eq. 29 contributes. One then obtains the result

$$\tilde{P}_n^+ = \langle|\tilde{A}_n^+|^2\rangle = \frac{1}{n!}\sum_{P,P'\in S_n} V_N(\tau)\,, \tag{30}$$

where $\tau = \mathcal{P}(\mathcal{P}')^{-1}$ is the target permutation of the scattering matrix correlator. Since τ is a product of two permutations, summing over the pair $\mathcal{P},\mathcal{P}'$ just means that τ covers the space of permutations $n!$ times and

$$\tilde{P}_n^+ = \sum_{\tau\in S_n} V_N(\tau)\,. \tag{31}$$

Since the class coefficients only depend on the cycle type of τ, one could rewrite the sum in terms of partitions. For this we let $\boldsymbol{v}$ be a vector whose elements v_l count the number of cycles of length l in τ so that $\sum_l l v_l = n$. Accounting for the number of ways to arrange the n elements in cycles, one can write the correlator as

$$\tilde{P}_n^+ = \sum_{\boldsymbol{v}}^{\sum_l l v_l = n} \frac{n! V_N(\boldsymbol{v})}{\prod_l l^{v_l} v_l!} \tag{32}$$

where we represent the argument of V by the cycles encoded in $\boldsymbol{v}$.

Typically, one considers correlators with a fixed target permutation, rather than sums over correlators as here in Eq. 31. For example fixing $\tau = (1,\dots,n)$ provides the linear transport moments while $\tau = id$ gives the moments of the conductance. A summary of some of the transport quantities which have been treated with RMT and semiclassics can be found in [38].

Examples

Representing the argument of the class coefficients V_N instead by its cycle type, one can directly write down the result for $n = 1, 2$:

$$\begin{aligned}\tilde{P}_1^+ &= V_N(1)\\ \tilde{P}_2^+ &= V_N(1,1) + V_N(2)\,,\end{aligned} \tag{33}$$

while for $n = 3$ there are 6 permutations

$$\begin{array}{lll} (1)(2)(3) & (123) & (132) \\ (1)(23) & (12)(3) & (13)(2)\,, \end{array} \tag{34}$$

and so

$$\tilde{P}_3^+ = V_N(1,1,1) + 3V_N(2,1) + 2V_N(3)\,. \tag{35}$$

With the recursive results in [37, 39] for the class coefficients we can easily find the following results for low n:

Unitary case

Without time reversal symmetry, the results are

$$\begin{aligned} \tilde{P}_1^+ &= \frac{1}{N} \\ \tilde{P}_2^+ &= \frac{1}{N(N+1)} \\ \tilde{P}_3^+ &= \frac{1}{N(N+1)(N+2)} \\ \tilde{P}_4^+ &= \frac{1}{N(N+1)(N+2)(N+3)} \\ \tilde{P}_5^+ &= \frac{1}{N(N+1)(N+2)(N+3)(N+4)}\,. \end{aligned} \tag{36}$$

The pattern seems to be

$$\tilde{P}_n^+ = \frac{\Gamma(N)}{\Gamma(N+n)}\,. \tag{37}$$

An inductive proof using Eq. 32 and recursive sums for the class coefficients should be possible. The expansion in N^{-1} would then be

$$\tilde{P}_n^+ = \frac{1}{N^n} - \frac{n(n-1)}{2N^{n+1}} + \ldots \tag{38}$$

Orthogonal case

With time reversal symmetry, the results are

$$\begin{aligned} \tilde{P}_1^+ &= \frac{1}{(N+1)} \\ \tilde{P}_2^+ &= \frac{1}{N(N+3)} \\ \tilde{P}_3^+ &= \frac{1}{N(N+1)(N+5)} \\ \tilde{P}_4^+ &= \frac{1}{N(N+1)(N+2)(N+7)} \\ \tilde{P}_5^+ &= \frac{1}{N(N+1)(N+2)(N+3)(N+9)}\,, \end{aligned} \tag{39}$$

suggesting a general result of

$$\tilde{P}_n^+ = \frac{\Gamma(N)}{\Gamma(N+n)}\frac{(N+n-1)}{(N+2n-1)}\,, \tag{40}$$

with an expansion of

$$\tilde{P}_n^+ = \frac{1}{N^n} - \frac{n(n+1)}{2N^{n+1}} + \ldots \tag{41}$$

Diagrammatic treatment without time reversal symmetry

For a given cycle $(1,\ldots,l)$ in the target permutation τ the semiclassical trajectories have a very particular structure whereby we first travel along a trajectory with positive action from i_1 to o_1 and then in reverse back along a trajectory with negative action to i_2 and so on along a cycle until we return to i_1. For example for $n = 3$ we have the trajectory connections in Fig. 5(a) for each target permutation τ in Eq. 34.

For the actions of the diagram to nearly cancel, and to obtain a semiclassical contribution, the trajectories must be nearly identical, except at small regions called encounters. By directly collapsing the trajectories onto each other, as in Fig. 5(b) we obtain some of the leading order diagrams for each τ. In fact for each diagram, following the rules of [40], the semiclassical contribution is a factor of $-N$ for each encounter and a factor of N^{-1} for each link between the encounters. For each cycle of length l in the diagrams in Fig. 5(b) one then has a factor of order N^{-2l+1}. One then needs to generate all permissible diagrams.

As shown in [36, 37] however the vast majority of semiclassical transport diagrams cancel. Those which remain can be untied until their target permutation becomes identity. For systems without time reversal symmetry, which we consider first, they can be mapped to primitive factorisations. One can reverse the process to build the diagrams by starting with a set of n independent links and tying together two outgoing channels into a new encounter. This tying process increases the order of the diagram by N^{-1}. If the outgoing channels are labelled by j and k then the target permutation also changes to $\tau(j\,k)$. For example going from the top left diagram of Fig. 5(b) tying together any two outgoing channels leads to the three example along the bottom row. The diagrams correspondingly move from order N^{-3} to N^{-4}.

Tying the remaining outgoing channel to one of those already tied leads to a diagram of the type further along the top row of Fig. 5(b) [for each of which there are 3 possible arrangements, and an alternative with a single larger encounter] and now of order N^{-5}.

Of course one could retie the same pair chosen in the first step, so that the target permutation is again identity. Such a diagram is however not shown in Fig. 5(b) but can be thought of as a higher order correction to a diagonal pair of trajectories. These types of diagrams appear when one treats the conductance variance for example. Such diagrams have a graphical interpretation which we will discuss below and use to generate them.

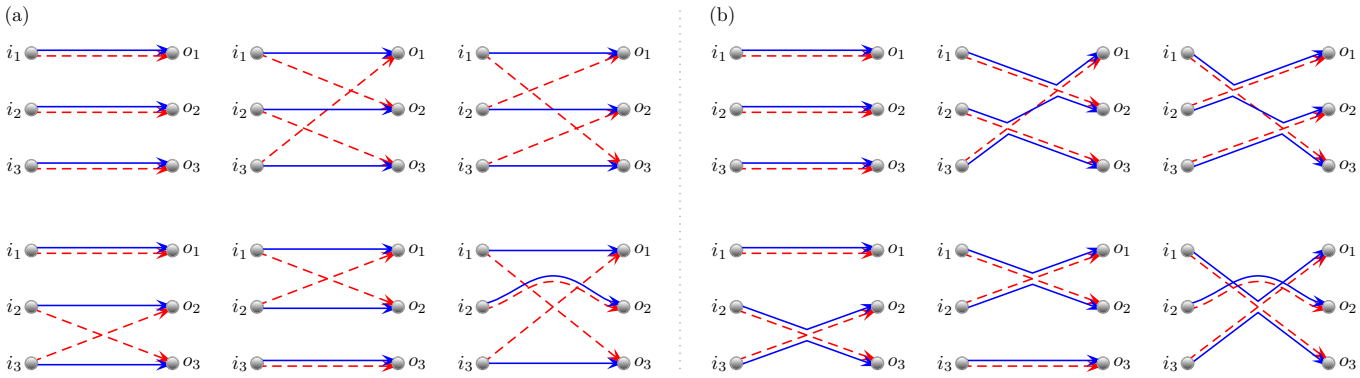

FIG. 5. (a) The permutations on 3 labels represented as trajectory diagrams. (b) Semiclassical contributions come when the trajectories are nearly identical, as when collapsed onto each other.

Forests

At leading order for each cycle of length l in τ the trajectories however form a ribbon graph in the shape of a tree. The tree has $2l$ leaves (vertices of degree 1) and all further vertices of even degree greater than 2. Such trees can be generated [41] by first treating unrooted trees whose contributions we store in the generating function f. Using the notation in [35], the function satisfies

$$f = \frac{r}{N} - \sum_{k=2}^{\infty} f^{2k-1}\,, \qquad \frac{f}{N} = \frac{\sqrt{1+\frac{4r^2}{N^2}}-1}{2r}\,, \tag{42}$$

where the power of r counts the number of leaves and the encounters may not touch the leads since the channels are distinct. Rooting the tree we add a leave to arrive at the generating function $F = rf$ while setting $r^2 = s$ we arrive at

$$\frac{F}{N} = \frac{\sqrt{1+\frac{4s}{N^2}}-1}{2}\,. \tag{43}$$

Expanding in powers of s

$$F = \frac{s}{N} - \frac{s^2}{N^3} + \frac{2s^3}{N^5} - \frac{5s^4}{N^7} + \frac{14s^5}{N^9} + \dots \tag{44}$$

one has an alternating sequence of Catalan numbers, A000108 [42].

When summing over all permutations for τ, each cycle of length l can be arranged in $(l-1)!$ ways and we now wish to include this factor in the ordinary generating function. First we divide instead by a factor l with the transformation

$$\frac{K_0}{N} = \int \frac{F}{sN}\,\mathrm{d}s = \sqrt{1+\frac{4s}{N^2}} - 1 + \frac{1}{2}\ln\left[\frac{N^4\left(1-\sqrt{1+\frac{4s}{N^2}}\right)}{2s^2} + \frac{N^2}{s}\right], \tag{45}$$

so that K_0 becomes the exponential generating function of the leading order trees multiplied by the factor $(l-1)!$ as required. To now generate any forest of trees corresponding to all permutations τ we can exponentiate K_0 to obtain the exponential generating function

$$\mathrm{e}^{K_0} - 1 = \frac{s}{N} + \frac{(N-1)s^2}{2N^3} + \frac{(N^2-3N+4)s^3}{6N^5} + \frac{(N^3-6N^2+19N-30)s^4}{24N^7} + \dots \tag{46}$$

whose first few terms can be explicitly checked against diagrams.

Higher order corrections to trees

For each given cycle $(1,\dots,l)$ of τ there are higher order (in N^{-1}) corrections which can be organised in a diagrammatic expansion [35, 38]. For systems without time reversal symmetry, the first correction occurs two orders lower than leading order and the corresponding diagrams can be generated by grafting the unrooted trees on two particular base diagrams. Repeating the steps in [35], while excluding the possibility for encounters to touch the leads (since the channels are distinct), one first obtains

$$K_2 = -\frac{(f^2+3)f^4}{6(f^2+1)^3}\,, \tag{47}$$

where handily, the method for subleading corrections automatically undercounts by a factor of l so we directly obtain the required exponential generating function. Finally we substitute from Eq. 42 and find

$$12NK_2 = \frac{1+\frac{6s}{N^2}}{\left(1+\frac{4s}{N^2}\right)^{\frac{3}{2}}} - 1\,. \tag{48}$$

The exponential generating function $\mathrm{e}^{K_0+K_2}-1$ would then generate all corresponding diagram sets up to this order.

Other corrections

However, the higher order corrections to trees are less important than the higher order corrections to other target permutation structures. For any pair of cycles $(1,\ldots,k)(k+1,\ldots,l)$ in τ we can have diagrams which are order N^{-2} smaller than a pair of leading order trees. For example, tying any two outgoing channels of a tree on the cycle $(1,\ldots,l)$ would break the target permutation into two as here.

To generate diagrams with two cycles, we graft trees around both sides of a circle as for the cross correlation of transport moments treated in [35]. This will include the example with $n = 3$ mentioned at the start of this subsection.

Following the steps in [35], while excluding the possibility of encounters touching the lead, one finds the generating function

$$\begin{aligned}\kappa = &-\ln\left[\frac{1-f_1^2f_2^2}{(1-f_1^2)^2(1-f_2^2)^2}\right] \\ &+\ln\left[\frac{1}{(1-f_1^2)^2}\right]+\ln\left[\frac{1}{(1-f_2^2)^2}\right],\end{aligned} \tag{49}$$

where f_1 and f_2 are the f in Eq. 42 but with arguments r_1 and r_2 respectively. The last two terms are corrections for when either r_1 or r_2 is 0 to remove diagrams with no trees on either side of the circle. In [35], κ was differentiated and such terms removed automatically, but here this correction simplifies the result to

$$\kappa = -\ln\left[1-f_1^2f_2^2\right]. \tag{50}$$

This generating function again undercounts by both a factor of k and $(l-k)$ and can therefore be thought of as an exponential generating function of both arguments. Setting $s_1 = s_2 = s$ then sums the possible splittings of the l elements into two cycles (along with the combinatorial factor of choosing the label sets), counting each splitting twice. This then provides the following exponential generating function

$$\begin{aligned}\kappa_1 &= -\frac{1}{2}\ln\left[1-f^4\right] \\ &= -\frac{1}{2}\ln\left[\frac{N^4}{2s^2}\left(\sqrt{1+\frac{4s}{N^2}}\left(1+\frac{2s}{N^2}\right)-1-\frac{4s}{N^2}\right)\right],\end{aligned} \tag{51}$$

whose expansion is

$$\kappa_1 = \frac{s^2}{2N^4}-\frac{2s^3}{N^6}+\frac{29s^4}{4N^8}-\frac{26s^5}{N^{10}}+\ldots \tag{52}$$

Order of contributions

With the diagrams treated so far the exponential generating function would be

$$\begin{aligned}\mathrm{e}^{K_0+\kappa_1+K_2}-1 = &\frac{s}{N}+\frac{(N^3-N^2+N-1)s^2}{2N^5} \\ &+\frac{(N^4-3N^3+7N^2-15N+20)s^3}{6N^7} \\ &+\ldots\end{aligned} \tag{53}$$

and the differences from Eq. 46 occur two orders lower in N^{-1} than the leading term from independent links. This is because the additional diagrams required at least two tying operations. However, we wish to know how the contributions change when n scales with N in some way.

First we can compare the contributions coming from K_2 to those from K_0. In the forest we can replace any tree from K_0 with its higher order correction in K_2. Since there can be at most n trees, and the correction is order N^{-2} smaller, these corrections will be bound by nN^{-2}, up to the scale of the generating function coefficients. This means that we can expect the contributions from K_2 to not be important when $n = O(N^2)$ as we take the limit $N \to \infty$.

Next we compare the contributions coming from κ_1 to those from K_0. In the forest we can now replace any tree by breaking its l cycle into two, say k and $(l-k)$. Alongside the generating function coefficients, the two new cycles come with the factor $(l-k-1)!(k-1)!$ instead of the $(l-1)!$ that was with the tree. Since

$$\begin{aligned}&\frac{1}{(l-1)!}\sum_{k=1}^{l-1} l-1\left(\begin{array}{c} l \\ k \end{array}\right)(l-k-1)!(k-1)! \\ &=\sum_{k=1}^{l-1}\frac{l}{(l-k)k} \leq l\,,\end{aligned} \tag{54}$$

this contribution is bound by nN^{-1} and should not be important when $n = O(N)$.

Continuing in this vein we could break up any tree into three cycles and generate those diagrams but this should also be higher order when $n \ll N$. Keeping our expansion to this order we should have

$$\begin{aligned}\mathrm{e}^{K_0+\kappa_1}-1 = &\frac{s}{N}+\frac{(N^2-N+1)s^2}{2N^4} \\ &+\frac{(N^3-3N^2+7N-12)s^3}{6N^6}+\ldots\end{aligned} \tag{55}$$

Time reversal symmetry

With time reversal symmetry, additional diagrams become possible. For example we may reverse the trajectories on one side of the circle used for cross correlations and obtain $2\kappa_1$ instead of just κ_1. There are also additional base diagrams at the second order correction to

trees, which may be treated as in [35], but which we do not treat here since there are now diagrams at the the first order correction. These can be generated by grafting trees around a Möbius strip. Following again the steps in [35] while excluding the possibility of encounters touching the lead one obtains the generating function

$$K_1 = \frac{1}{2}\ln\left[\frac{1-f^2}{1+f^2}\right], \tag{56}$$

or explicitly

$$\begin{aligned} K_1 &= -\frac{1}{4}\ln\left[1+\frac{4s}{N^2}\right] \\ &= -\frac{s}{N^2}+\frac{2s^2}{N^4}-\frac{16s^2}{3N^6}+\frac{16s^4}{N^8}-\frac{256s^5}{5N^{10}}+\dots \end{aligned} \tag{57}$$

Compared to the leading order forest, we could replace any tree by its higher order correction and obtain a term bound by nN^{-1}, again up to the scale of the generating function coefficients. Restricting to $n = O(N)$ the the exponential generating function would be

$$\begin{aligned} \mathrm{e}^{K_0+2\kappa_1+K_1}-1 = &\frac{(N-1)s}{N^2}+\frac{(N^2-3N+7)s^2}{2N^4} \\ &+\frac{(N^3-6N^2+28N-75)s^3}{6N^6} \\ &+\dots \end{aligned} \tag{58}$$

Fermions

For n fermions we start instead with

$$\tilde{A}_n^- = \frac{1}{\sqrt{n!}}\sum_{\mathcal{P}\in S_n}(-1)^{\mathcal{P}}\prod_{k=1}^{n} Z_{i_k,o_{\mathcal{P}(k)}}, \tag{59}$$

where $(-1)^{\mathcal{P}}$ represents the sign of the permutation, counting a factor of -1 for each even length cycle in $\mathcal{P}$. Following the same steps for bosons, one has

$$\tilde{P}_n^- = \langle|\tilde{A}_n^-|^2\rangle = \sum_{\tau\in S_n}(-1)^{\tau}V_N(\tau), \tag{60}$$

so for example

$$\tilde{P}_3^- = V_N(1,1,1)-3V_N(2,1)+2V_N(3). \tag{61}$$

Calculating the class coefficients recursively one then finds the following results for low n:

Unitary case

Without time reversal symmetry, the results are

$$\begin{aligned} \tilde{P}_1^- &= \frac{1}{N} \\ \tilde{P}_2^- &= \frac{1}{N(N-1)} \\ \tilde{P}_3^- &= \frac{1}{N(N-1)(N-2)} \\ \tilde{P}_4^- &= \frac{1}{N(N-1)(N-2)(N-3)} \\ \tilde{P}_5^- &= \frac{1}{N(N-1)(N-2)(N-3)(N-4)}, \end{aligned} \tag{62}$$

The pattern seems to be

$$\tilde{P}_n^- = \frac{\Gamma(N-n+1)}{\Gamma(N+1)}, \tag{63}$$

and the expansion in N^{-1} would then be

$$\tilde{P}_n^- = \frac{1}{N^n}+\frac{n(n-1)}{2N^{n+1}}+\dots \tag{64}$$

Orthogonal case

With time reversal symmetry, the results are

$$\begin{aligned} \tilde{P}_1^- &= \frac{1}{(N+1)} \\ \tilde{P}_2^- &= \frac{1}{(N+1)N} \\ \tilde{P}_3^- &= \frac{1}{(N+1)N(N-1)} \\ \tilde{P}_4^- &= \frac{1}{(N+1)N(N-1)(N-2)} \\ \tilde{P}_5^- &= \frac{1}{(N+1)N(N-1)(N-2)(N-3)} \end{aligned} \tag{65}$$

suggesting a general result of

$$\tilde{P}_n^- = \frac{\Gamma(N-n+2)}{\Gamma(N+2)} \tag{66}$$

with an expansion of

$$\tilde{P}_n^+ = \frac{1}{N^n}+\frac{n(n-3)}{2N^{n+1}}+\dots \tag{67}$$

Generating functions

However, because our semiclassical generating functions are organised by cycle type, we simply need to replace s by $-s$ and multiply the K type functions by -1 appropriately.

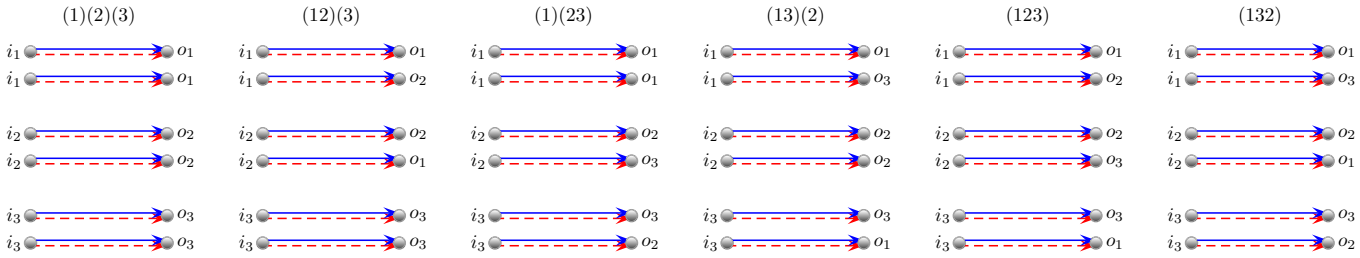

FIG. 6. The leading order diagrams for the variance with 3 particles are created by finding semiclassical diagrams with 6 incoming and outgoing channels. When the channels coincide, the leading order diagrams must reduce to separated links corresponding to one of the permutations on 3 labels depicted.

The variance

Now for n bosons we look at

$$|\tilde{A}_n^+|^4 = \frac{1}{(n!)^2} \sum_{\substack{\mathcal{P},\mathcal{P}' \\ \mathcal{R},\mathcal{R}' \in S_n}} \prod_{k=1}^{n} Z_{i_k,o_{\mathcal{P}(k)}} Z^*_{i_k,o_{\mathcal{P}'(k)}} \times Z_{i_k,o_{\mathcal{R}(k)}} Z^*_{i_k,o_{\mathcal{R}'(k)}} \,, \tag{68}$$

or rather the average

$$L_n^+ = \left\langle |\tilde{A}_n^+|^4 \right\rangle \,. \tag{69}$$

However, when we now compare to Eq. 29 such an average involves summing over permutations of length $2n$ while each of the originally distinct channels appears exactly twice. For example

$$L_1^+ = \langle Z_{i_1,o_1} Z_{i_1,o_1} Z^*_{i_1,o_1} Z^*_{i_1,o_1} \rangle = 2V_N(1,1) + 2V_N(2) \,, \tag{70}$$

since the delta function conditions in Eq. 29 are satisfied for any choice of σ and π. The result is

$$L_1^+ = \frac{2}{N(N+1)} \qquad L_1^+ = \frac{2}{N(N+3)} \,, \tag{71}$$

without or with time reversal symmetry respectively.

For $n = 2$, we can run through the sums of permutations, giving

$$L_2^+ = \frac{3N^2 - N + 2}{N^2(N^2-1)(N+2)(N+3)} \,, \tag{72}$$

without time reversal symmetry and

$$L_2^+ = \frac{3N^2 + 5N - 16}{N(N^2-4)(N+1)(N+3)(N+7)} \,, \tag{73}$$

with. For large n this process however quickly becomes computationally intractable. Diagrammatically, we can imagine multiplying the sets of diagrams we had before, but also keeping track of all the possible permutations and which channels coincide. For example we could take the diagrams in Fig. 5(b), add the remaining 5 copies of each diagram created by permuting the outgoing labels, and multiply the entire set by itself to obtain pairs of diagrams which appear for the variance. Of course each pair is over counted $(n!)^2$ times and we would still need to account for the diagrams where the pairs interact and where the repeated channels play a role by considering diagrams acting on $2n$ leaves.

To reduce the difficulty of such a diagrammatic expansion, we focus here instead on just calculating the leading order term. We know that these terms are represented diagrammatically by sets of independent links so we select the $(n!)^2$ such sets from our multiplication. Since each outgoing channel (although appearing twice) is distinct we may relabel them appropriately to reduce our leading order diagrams to $n!$ ways of permuting a single outgoing label. The sum of a product of two permutations essentially reduces to a sum over a single permutation. The overcounting is now $n!$ instead. For $n = 3$ the leading order diagrams are depicted in Fig. 6. For each diagram we have the standard leading order result of N^{-2n} which, when dividing by the over counting, would be the total result if the outgoing channels were different.

However, for each cycle of the effective permutation of the outgoing channels, an additional semiclassical diagram is possible. By adding a 2-encounter to each pair of identical channels we can separate them into two artificially distinct channels. The resulting semiclassical diagram can be drawn as a series of 2-encounters around a circle with one link on either side. This process is depicted in Fig. 7. The resulting starting point is from the larger set of possible trajectory correlators than just the sets of independent links squared, but once we move all the encounters into the appropriate leads, the required channels coincide and we have an additional leading order diagram.

To count such possibilities we just need to include a power of 2 for each cycle in the permutation of the outgoing channels when we include the standard diagonal terms. For each cycle of length l there are $(l-1)!$ different permutations so that

$$-2\log(1-s) = 2s + s^2 + \frac{2s^3}{3} + \frac{s^4}{2} + \ldots \tag{74}$$

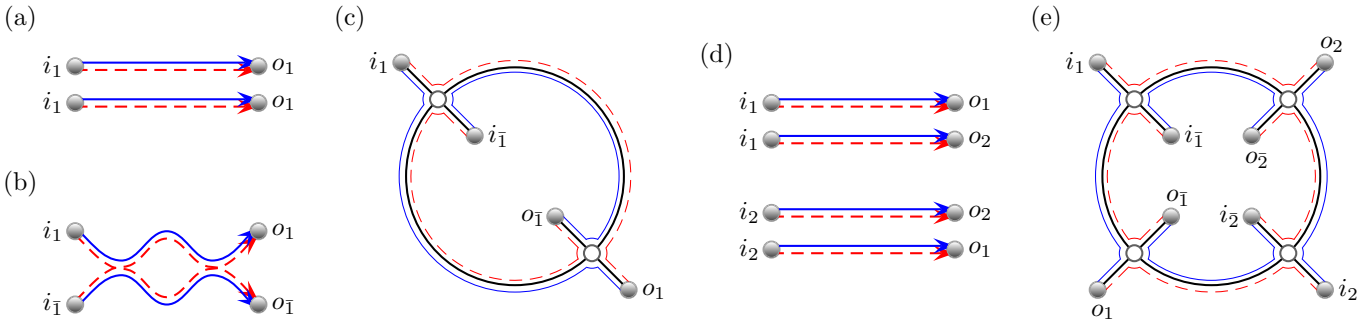

FIG. 7. (a) A pair of independent links can be joined by an encounter at each end to create the diagram in (b) with artificially distinct incoming and outgoing channels. When the encounters are moved into the incoming and outgoing leads respectively, the channels again coincide leading to a new leading order semiclassical diagram. In the graphical representation, the trajectories in (b) become the boundary walks around both sides of the circle in (c). Starting with four links corresponding to the permutation (12) in (d) we can create the correlated quadruplet represented in (e). Again moving the encounters into the leads creates a new leading order contribution.

acts as the exponential generating function of both possibilities for each cycle times their number of permutations. To generate all leading order diagrams we simply exponentiate this function

$$\mathrm{e}^{-2\log(1-s)} - 1 = \frac{1}{(1-s)^2} - 1 \tag{75}$$

Since we are still overcounting by $n!$ this actually provides the ordinary generating function and when we include the semiclassical contributions of N^{-2n} we get the final leading order result of

$$L_n^+ = \frac{n+1}{N^{2n}} + O(N^{-2n+1}) \tag{76}$$

or a variance of

$$L_n^+ - \left(\tilde{P}_n^+\right)^2 = \frac{n}{N^{2n}} + O(N^{-2n+1}) \tag{77}$$

We checked this against the explicit semiclassical or RMT results involving Eq. 29 for n up to 5. Since the semiclassical diagrams all involve pairs of equally long cycles, the leading order result is also the same for fermions.

Intriguingly, the numerator of the leading order result for the second moments in Eq. 76 is identical to the second moment of the modulus squared of the permanents of $n \times n$ random complex Gaussian matrices [43]. Higher moments of such permanents would be useful to determine the validity of the *Permanent Anti-Concentration Conjecture* important for Boson Sampling [43]. This opens the possibility that a semiclassical or RMT treatment of the higher moments of many body scattering, expanded just to leading order, could help answer such questions.

[35] G. Berkolaiko and J. Kuipers, *New J. Phys.* **13**, 063020 (2011).

[36] G. Berkolaiko and J. Kuipers, *Phys. Rev. E* **85**, 045201 (2012).

[37] G. Berkolaiko and J. Kuipers, *J. Math. Phys.* **54**, 112103 (2013).

[38] G. Berkolaiko and J. Kuipers, *J. Math. Phys.* **54**, 123505 (2013).

[39] P. W. Brouwer and C. W. J. Beenakker, *J. Math. Phys.* **37**, 4904- (1996).

[40] S. Müller, S. Heusler, P. Braun, and F. Haake, *New J. Phys.* **9**, 12 (2007).

[41] G. Berkolaiko, J. M. Harrison, and M. Novaes, *J. Phys. A* **41**, 365102 (2008).

[42] N. J. A. Sloane, The on-line encyclopedia of integer sequences, published electronically at http://www.research.att.com/∼njas/sequences/

[43] S. Aaronson and A. Arkhipov, *Theory Comp.* **9**, 143- (2013).